DISEASES AND DISORDERS

Epigenetic transcriptional reprogramming by WT1 mediates a repair response during podocyte injury

Sandrine Ettou[1,2]*, Youngsook L. Jung[3]*, Tomoya Miyoshi[4,5,6†], Dhawal Jain[3†], Ken Hiratsuka[4,5,6,7], Valerie Schumacher[1,2], Mary E. Taglienti[1], Ryuji Morizane[4,5,6,7,8], Peter J. Park[3,8‡], Jordan A. Kreidberg[1,2,8‡]

In the context of human disease, the mechanisms whereby transcription factors reprogram gene expression in reparative responses to injury are not well understood. We have studied the mechanisms of transcriptional reprogramming in disease using murine kidney podocytes as a model for tissue injury. Podocytes are a crucial component of glomeruli, the filtration units of each nephron. Podocyte injury is the initial event in many processes that lead to end-stage kidney disease. Wilms tumor-1 (WT1) is a master regulator of gene expression in podocytes, binding nearly all genes known to be crucial for maintenance of the glomerular filtration barrier. Using murine models and human kidney organoids, we investigated WT1-mediated transcriptional reprogramming during the course of podocyte injury. Reprogramming the transcriptome involved highly dynamic changes in the binding of WT1 to target genes during a reparative injury response, affecting chromatin state and expression levels of target genes.

INTRODUCTION

Many studies have used transcriptional profiling to identify changes in the transcriptome during the progression of human disease. However, very few studies have identified the mechanisms whereby specific transcription factors (TFs) respond to the incipient cellular injury events that occur at the onset of disease. To study the regulation of transcriptional responses during cellular injury, we have used as a model the Wilms tumor-1 (WT1) TF and its role in responding to cellular injury in kidney podocytes. Podocytes are a key cell type in kidneys, injury to which leads to many causes of human nephrotic syndrome, a highly compromised state in which there is massive loss of protein in the urine, leading to severe edema and the requirement for dialysis or kidney transplant for survival. Focal segmental glomerulosclerosis (FSGS) is among the most debilitating and least treatable forms of human nephrotic syndrome and often leads to end-stage kidney disease, requiring dialysis and/or transplantation. Podocytes are highly differentiated cells that maintain the glomerular filtration barrier (GFB) through the extension of foot processes that interdigitate with foot processes of adjacent podocytes, thereby assembling a scaffold that supports a network of capillaries within each glomerulus. In most types of FSGS, podocyte injury is the first cellular injury event in the kidney (*1*), characterized by foot process effacement and podocyte detachment, resulting in loss of the GFB and severe proteinuria (*2*). Several proteins are implicated in maintaining podocyte structural organization, including synaptopodin, nephrin, and podocin. One common characteristic of glomerular injury is the decreased abundance of key proteins that maintain the GFB, suggesting that transcriptional regulation of genes encoding these proteins has an important role in the pathogenesis of glomerular disease.

Our previous study and others identified WT1 as one of the most upstream TFs regulating gene expression in podocytes (*3*, *4*) and one of the earliest known markers of podocytes during kidney development (*5*). Decreased expression of *WT1* and mutations in *WT1* gene have been described in several forms of glomerular disease (*6*–*10*). Most human nephrotic syndrome genes have been identified as WT1 targets, including *NPHS1*, *NPHS2*, and *INF2* (*4*). However, the mechanism whereby WT1 regulates gene expression during the initiation and progression of glomerular disease remains unknown.

In the present study, we focused on deciphering the transcriptional mechanisms through which WT1 regulates podocyte gene expression during injury. Genome-wide analysis of both WT1 DNA occupancy and podocyte gene expression during the course of adriamycin (ADR)–mediated injury revealed a transient increase in the number and binding intensity [defined as peak height in chromatin immunoprecipitation sequencing (ChIP-seq) datasets] of WT1-bound sites and an increase in the expression of crucial podocyte genes at early stages of injury, which may reflect an attempt to repair podocytes. We demonstrated that WT1 is required to maintain active chromatin marks at podocyte genes and that podocyte injury leads to the conversion from active to repressive histone modifications at *Nphs2* and *Synpo*. Together, this study provides strong evidence that, during injury, podocyte gene expression is subject to transcriptional reprogramming under the direct control of WT1, indicating that podocytes have an intrinsic repair program acting at the level of gene expression.

RESULTS

WT1 mediated epigenetic regulation in podocytes

WT1 has been identified as a key regulator of podocyte gene expression (*3*, *4*), and WT1 target genes are crucial for maintaining GFB (*4*, *11*). Two WT1 target genes were studied to elucidate the transcriptional response to injury. First, *Nphs2* encodes podocin, an essential component of the slit diaphragm, a cell-cell junctional

[1]Department of Urology, Boston Children's Hospital, Boston, MA 02115, USA. [2]Department of Surgery, Harvard Medical School, Boston, MA 02115, USA. [3]Department of Biomedical Informatics, Harvard Medical School, Boston, MA 02115, USA. [4]Nephrology Division, Massachusetts General Hospital, Boston, MA 02114, USA. [5]Renal Division, Brigham and Women's Hospital, Boston, MA 02115, USA. [6]Department of Medicine, Harvard Medical School, Boston, MA 02115, USA. [7]Wyss Institute for Biologically Inspired Engineering, Boston, MA 02115, USA. [8]Harvard Stem Cell Institute, Cambridge, MA 02138, USA.
*These authors contributed equally to this work.
†These authors contributed equally to this work.
‡Corresponding author. Email: jordan.kreidberg@childrens.harvard.edu (J.A.K.); peter_park@hms.harvard.edu (P.J.P.)

structure between adjacent podocytes, which is one of the most important components of the barrier that prevents proteins from leaving the circulation during filtration. The second gene, *Synpo*, encodes synaptopodin, an actin-associated protein important for maintaining podocyte cytoskeleton integrity. To directly demonstrate WT1-dependent gene expression, *Wt1* was conditionally inactivated in podocytes (*12*) of adult *Nphs2-CreERT2*, *WT1fl/fl* mice, leading to massive proteinuria (Fig. 1A). Kidneys appeared pale (Fig. 1B) with hematoxylin and eosin and periodic acid–Schiff staining, showing protein casts, mesangial expansion, and dilated tubules (Fig. 1C). WT1, podocin, and synaptopodin transcript and protein levels were greatly reduced (Fig. 1, D and E).

Tissue-specific TFs activate gene expression, in part, by promoting histone modifications that maintain open chromatin, such as H3K4me3 and H4K8ac. We used fluorescence-activated cell sorting (FACS)–isolated podocytes to analyze the effect of WT1 inactivation on histone modifications during the course of injury at previously defined WT1 binding sites at the *Nphs2* and *Synpo* genes (*4*), here identified as Nphs2-1, Nphs2-2, Nphs2-3, Synpo-1, Synpo-2, and Synpo-3. Nphs2-1 and Nphs2-2 are located upstream of the promoter and are putative enhancers. Nphs2-3 is at the transcriptional start site (TSS). Synpo-1 and Synpo-2 are located in intronic regions, and Synpo-3 overlaps the second exon (Fig. 1F). H3K4me3 and H4K8ac were greatly reduced after inactivation of WT1 at these sites (Fig. 1G), and the repressive histone marks H3K9me3 and H3K27me3 were increased (Fig. 1G), confirming that WT1 maintains the active chromatin state at target sites, thereby inhibiting the placement of repressive marks on histones (*13*). Similar results were observed in vitro with immortalized podocytes (fig. S1, A and B), demonstrating that WT1 has a crucial role in maintaining the open chromatin state at its target genes in podocyte.

Transient increase of podocyte gene expression in ADR-injured mice and human organoids

To analyze WT1-mediated transcriptional reprogramming during the course of injury, we used the ADR model for podocyte injury, a well-recognized murine model for FSGS (*14*). Two different strains of mice were used in this study: *mTmG-Nphs2cre* mice that are less sensitive to ADR, from which podocytes may be isolated by FACS, and BALB/cJ, a prototypical highly ADR-sensitive strain (*15*). To determine the time course of ADR-induced podocyte injury, we first analyzed the level of proteinuria of *mTmG-Nphs2cre* and BALB/cJ mice treated with either ADR or phosphate-buffered saline (PBS) as a control vehicle. *mTmG-Nphs2cre* mice required a higher dose and a second injection to develop maximal proteinuria after 2 weeks (Fig. 2A), whereas ADR induced proteinuria in BALB/cJ mice over a 1-week period (fig. S2A). The expression of WT1 has previously been shown to decrease after the onset of glomerular disease (*16*). However, in BALB/cJ-isolated glomeruli, we observed a several-fold increase in *Wt1* expression after ADR treatment, before *Wt1* fell to low levels (fig. S2B). Concomitant with the transient increase in *Wt1*, *Nphs2* and *Synpo* also markedly increased before falling to nearly undetectable levels (fig. S2B). Although in *mTmG-Nphs2cre* FACS-isolated podocytes *Wt1* and *Nphs2* levels did not increase to the extent observed in BALB/cJ after ADR, *Synpo* did show an over twofold increase, suggesting that while less marked, there also appeared to have been transcriptional reprogramming mediated by WT1 in these mice (Fig. 2B). In *mTmG-Nphs2cre* mice, WT1 protein levels fell at day 9 (D9) after ADR. Podocin showed a slight increase, whereas synaptopodin showed an over threefold increase at D5 after ADR and then fell markedly (Fig. 2C). By immunofluorescent detection, WT1 was also present in podocyte nuclei until D5 in *mTmG-Nphs2cre* and D3 in BALB/cJ, after which it was decreased (Fig. 1D and fig. S2C). The expression of WT1 targets nephrin, synaptopodin, and podocalyxin, detected by coimmunofluroescent staining with WT1, was also greatly diminished by D14. Staining for green fluorescent protein (GFP), albeit diminished, demonstrated the presence of podocytes through the time frame of injury (Fig. 2D).

We next investigated the effect of ADR on organoids derived from human embryonic stem cells (hESCs). In addition to *WT1*, *NPHS2*, and *SYNPO*, we also examined *NPHS1,* encoding the slit diaphragm protein nephrin, because of its importance in genetic kidney disease. We observed similar transient increases in WT1 and target genes (Fig. 2, E to G). Although transcript levels continued to be expressed through D4 (Fig. 2E), protein levels for WT1, synaptopodin, nephrin (immunofluorescence only), and podocin were greatly decreased starting from D4 by either Western blot or immunofluorescent detection (Fig. 2, F and G). Podocalyxin, a glycocalyx sialoprotein located at the apical and lateral surface of podocytes, could be detected, albeit at lower levels, through D10, confirming their presence of podocytes throughout the injury process (Fig. 2G). Therefore, human podocytes also respond to injury by transiently increasing expression of WT1 and target genes, thus validating human kidney organoids as a model to study glomerular injury. Since protein levels did not precisely overlap with maximal RNA levels, there may also be translational regulation affecting their expression during injury. Nevertheless, the decrease in WT1 and target gene expression demonstrated substantial transcriptional reprogramming during the course of the injury.

Dynamics of WT1 occupancy during ADR-induced injury

The overall level of WT1 in podocytes may not be representative of its binding at specific enhancers or TSSs. The pattern of WT1 binding was distinct at each site (shown in Fig. 3D) for *Nphs2* and *Synpo* genes during injury (Fig. 3A). In *mTmG-Nphs2cre* mice, the most significant changes were increased binding at Nphs2-1 at D10 and decreased binding at Nphs2-3 after D5. Binding at all three *Synpo* sites transiently increased before falling to levels below those observed in uninjured mice, correlating with gene expression. This response is more marked in BALB/cJ mice, consistent with their greater sensitivity to ADR (fig. S2D).

Chromatin remodeling during ADR-induced injury

As WT1 occupancy maintains open chromatin and ADR results in loss of WT1 binding at target genes (Fig. 1F), we interrogated histone modifications at WT1 binding sites after ADR treatment (Fig. 3B). All WT1 binding sites were converted to closed chromatin state at D14 after ADR injury (Fig. 3B). H3K4me1, which marks active enhancers and promoters, was increased at WT1 binding sites at D9 (Fig. 3C), correlating with increased binding of WT1. H3K27ac, which marks active enhancers, was also increased at D9, except at the Nphs2-3 site present within a TSS (Fig. 3C). Similar results were observed in vitro (fig. S1, C and D). Thus, ADR-induced cellular injury initially results in an enhanced open chromatin state at WT1 target genes, followed by a conversion from an open to closed chromatin state at genes required to maintain normal cell function.

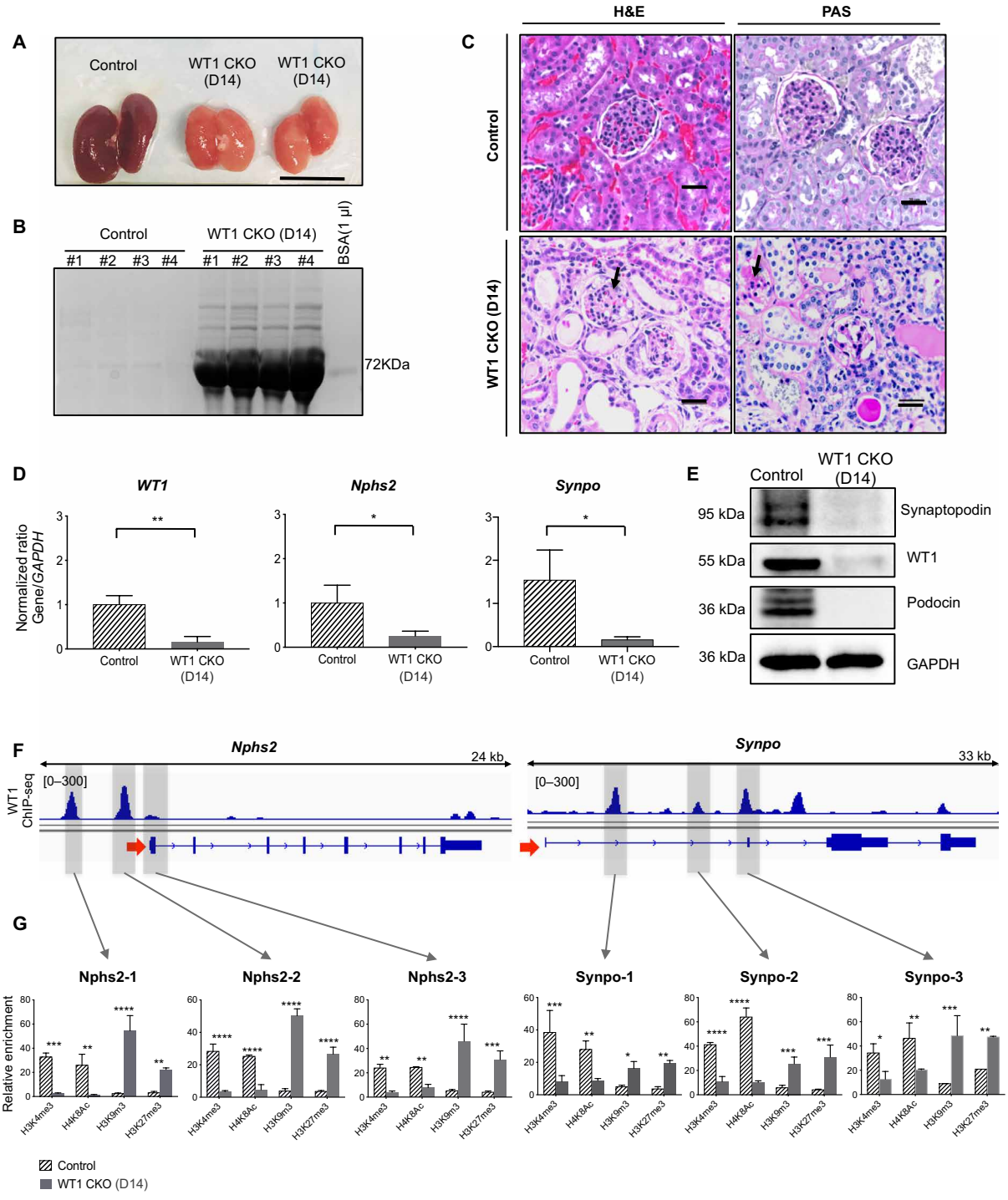

Fig. 1. WT1 controls chromatin remodeling at *Nphs2* and *Synpo* genes in mice. (**A**) *WT1*$^{flox/flox}$*/iNphs2-cre* mice exhibit smaller and pale kidneys compared to control ($n = 3$) at D14 after tamoxifen injection. Scale bar, 1 cm. (**B**) Coomassie stains gel of 5 µl of urine from *WT1*$^{flox/flox}$ (control) mice and *WT1*$^{flox/flox}$*/iNphs2-cre* (WT1 CKO) mice [control, bovine serum albumin (BSA)]. (**C**) Representative histological images of control and WT1 CKO kidneys by hematoxylin and eosin (H&E) and periodic acid–Schiff (PAS) at D14 after tamoxifen injections. Original magnification, ×60. Scale bars, 20 µm. Black arrows: mesengial expansion. (**D**) Reverse transcription quantitative polymerase chain reaction (RT-qPCR) of *Wt1*, *Nphs2*, and *Synpo* from isolated glomeruli of control and WT1 CKO mice. Bars represent means and error bars ± SEMs. $^{**}P < 0.01$ and $^{*}P < 0.05$ ($n = 3$). (**E**) Representative Western blot (of three independent experiments) from isolated glomeruli, reflecting WT1 expression from control and WT1 CKO mice at D14 after tamoxifen injections. (**F**) Integrative Genomics Viewer (IGV) plots of *Nphs2* and *Synpo* genes for WT1 ChIP-seq, showing WT1 binding sites (gray highlighted boxes) in uninjured podocytes: Nphs2-1, Nphs2-2, Nphs2-3, Synpo-1, Synpo-2, and Synpo-3. (**G**) Histone direct ChIP-qPCR from FACS-isolated podocytes from control and WT1 CKO mice 14 days after tamoxifen injections, using active histone marks (H3K4m3 and H4K8ac) and repressive histone marks (H3K9me3 and H3K27me3). $^{****}P < 0.0001$, $^{***}P < 0.001$, $^{**}P < 0.01$, and $^{*}P < 0.05$ [multiple *t* tests with false discovery rate (FDR) determined using the two-stage linear step-up procedure of Benjamini, Krieger, and Yekutieli] compared to control mice. GAPDH, glyceraldehyde-3-phosphate dehydrogenase. Photo credit for (A): Sandrine Ettou, Boston Children's Hospital.

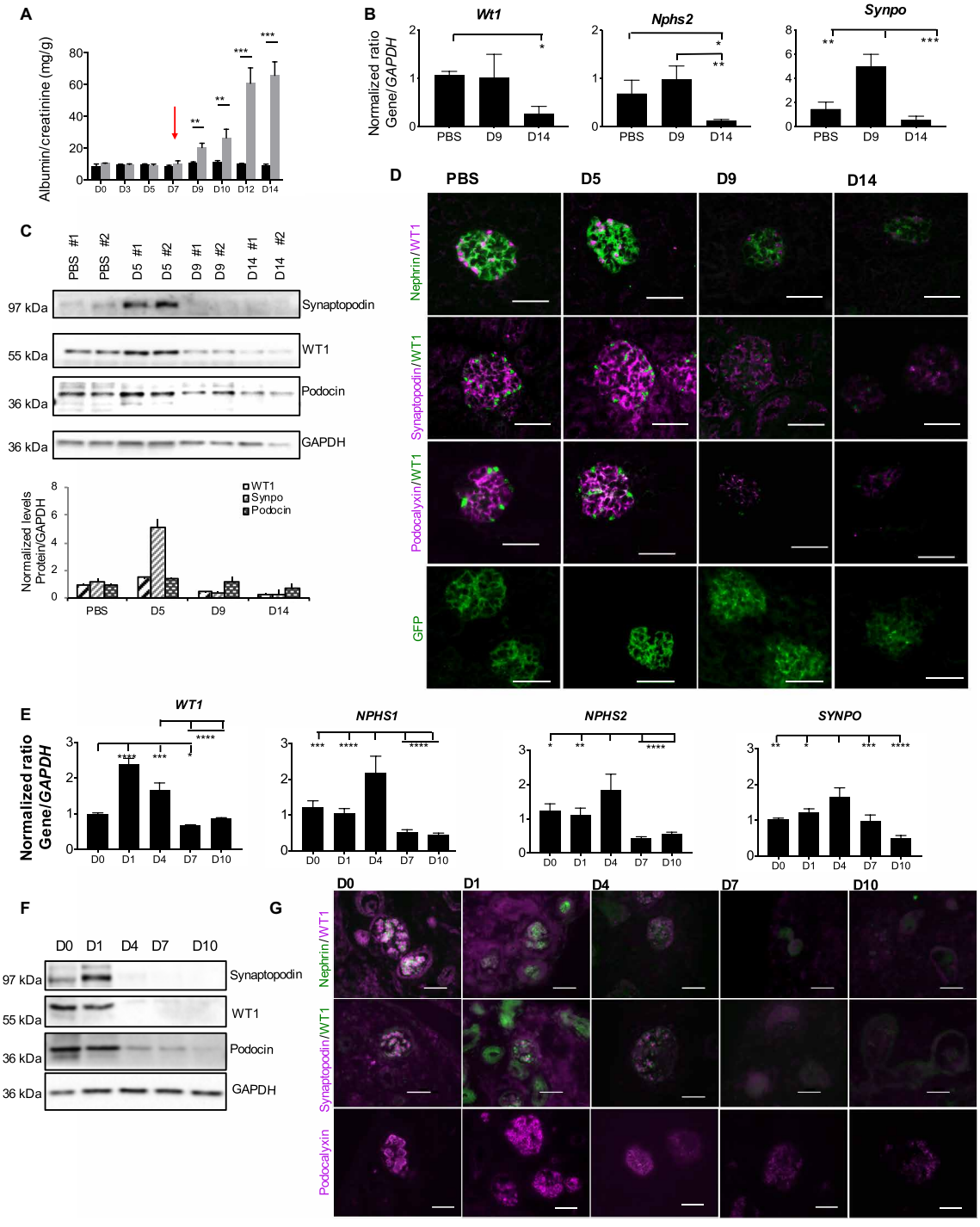

Fig. 2. Transient increase in the expression of key podocyte genes in ADR-injured mice and human organoids. (**A**) Quantification of albumin/creatinine level during the course of ADR injury from *mTmG-Nphs2cre* mice injected twice with ADR (18 mg/kg; gray bars) or PBS (black bars) at 1-week intervals (second injection indicated by red arrow). Bars represent means and error bars ± SEMs. ***$P < 0.001$ and **$P < 0.01$ ($n = 3$ replicates). (**B**) RT-qPCR of *Wt1*, *Nphs2*, and *Synpo* from *mTmG-Nphs2cre* FACS-isolated podocytes during injury. One-way analysis of variance (ANOVA) with Tukey's multiple comparisons test was used. ***$P < 0.001$, **$P < 0.01$. and *$P < 0.05$ ($n = 3$ replicates). (**C**) Representative Western blot (of three independent experiments performed) reflecting podocyte protein levels during the course of ADR-induced injury from *mTmG-Nphs2cre*–isolated glomeruli. Lower panel: quantification of Western blot based on $n = 3$. (**D**) Immunofluorescent staining of WT1, nephrin, synaptopodin, podocalyxin, and enhance green fluorescent protein (eGFP) in *mTmG-Nphs2cre* mice in glomeruli. The time point is at the top of each column. Scale bars, 50 μm. (**E**) RT-qPCR of *WT1*, *NPHS1*, *NPHS2*, and *SYNPO* from human kidney organoids treated with 10 μM ADR during 1, 4, 7, and 10 days. ANOVA with Tukey's multiple comparisons test was used. ****$P < 0.0001$, ***$P < 0.001$, **$P < 0.01$, and *$P < 0.05$ ($n = 3$). (**F**) Representative Western blot (of three independent experiments performed) reflecting podocyte protein levels during the course of ADR-induced injury from human kidney organoids. (**G**) Immunofluorescent localization of WT1, NPHS1, and podocalyxin at D0, D1, D4, D7, and D10 after treatment of human kidney organoids with ADR. Scale bars, 50 μm.

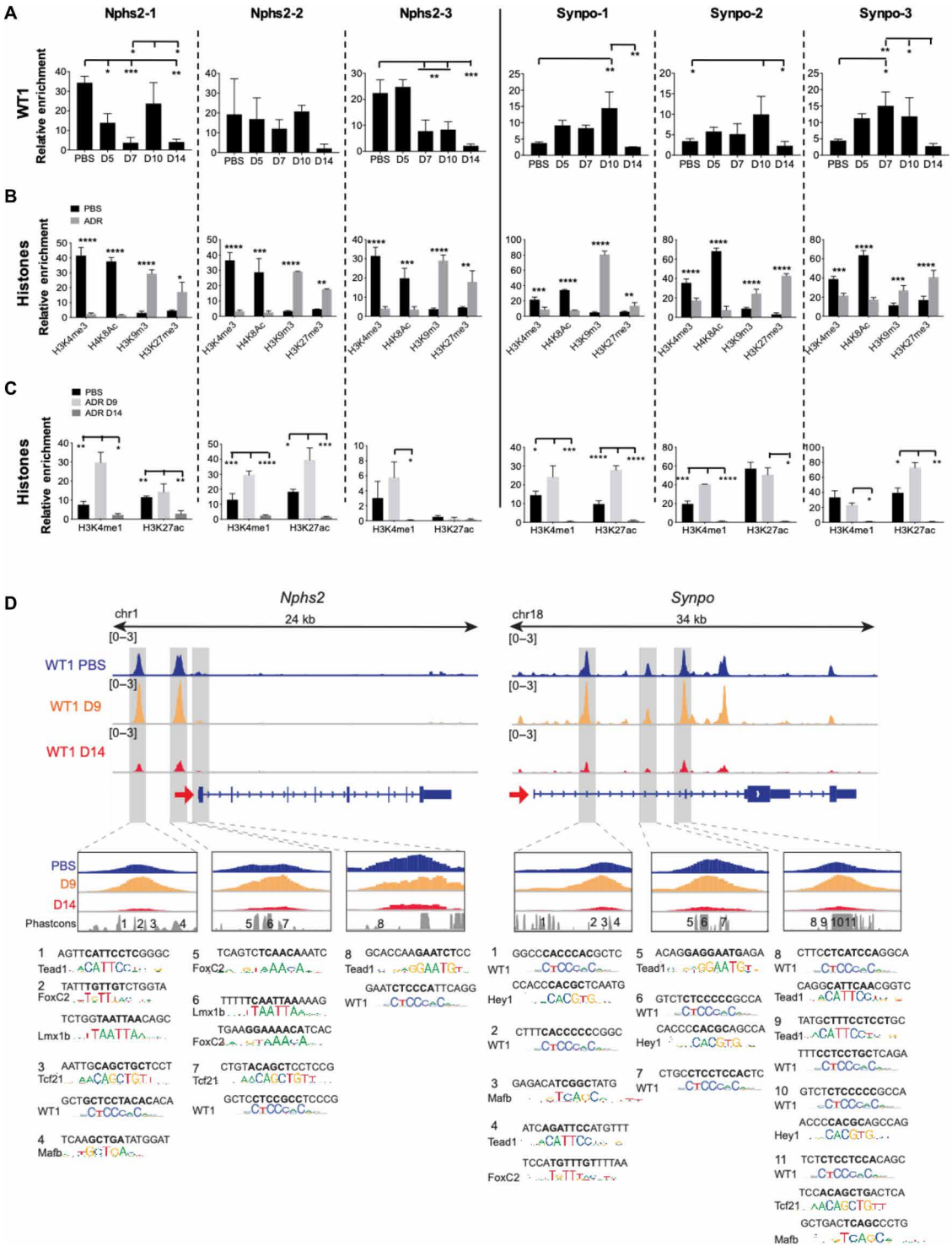

Fig. 3. Effect of WT1 dynamic binding on chromatin remodeling during ADR-induced injury in *mTmG-Nphs2cre* mice. (**A**) WT1 dynamic binding at three binding sites of *Nphs2* and *Synpo* genes measured by WT1 direct ChIP-qPCR from isolated glomeruli from *mTmG-Nphs2cre* mice ($n = 3$). ANOVA with Tukey's multiple comparisons test was used. ***$P < 0.001$, **$P < 0.01$, and *$P < 0.05$. (**B**) Histone direct ChIP-qPCR at D14 from FACS-isolated podocytes from *mTmG-Nphs2cre* mice, using active histone marks (H3K4m3 and H4K8ac) and repressive histone marks (H3K9me3 and H3K27me3; $n = 3$). ****$P < 0.0001$, ***$P < 0.001$, **$P < 0.01$, and *$P < 0.05$ (multiple t tests with FDR determined using the two-stage linear step-up procedure of Benjamini, Krieger, and Yekutieli) compared to uninjured mice. (**C**) Histone direct ChIP-qPCR at D9 and D14 from FACS-isolated podocytes from *mTmG-Nphs2cre* mice using active enhancer marks (H3K4m1 and H3K27ac; $n = 3$). ANOVA with Tukey's multiple comparisons test was used. ****$P < 0.0001$, ***$P < 0.001$, **$P < 0.01$, and *$P < 0.05$. (**D**) WT1 ChIP-seq profiles at *Nphs2* and *Synpo* genes during injury and predicted TF binding sites. Upper panels: IGV plots of WT1 binding at different sites during injury (uninjured, blue; D9, orange; D14, red). Red arrows show TSSs and direction of transcription. Gray highlighted boxes indicate WT1 binding sites shown in Fig. 1F. Lower panels: TF motifs identified within the numbered conserved elements.

Genome-wide dynamics of WT1 binding during injury

To identify general mechanisms through which WT1 regulates gene expression during the course of ADR-induced podocyte injury, we performed WT1 ChIP-seq using isolated glomeruli from *mTmG-Nphs2cre* and BALB/cJ mice and RNA sequencing (RNA-seq) using FACS-isolated podocytes from *mTmG-Nphs2cre* mice obtained at the onset of proteinuria (D9) and at a point of maximal proteinuria (D14; Fig. 1A). In *mTmG-Nphs2cre* mice, the global number of WT1-bound sites increased from 23,163 in control mice to 31,639 at D9 before falling markedly to 6567 binding sites at D14 (Fig. 4A). A total of 11,266 binding sites were uniquely present at D9 (Fig. 4A). Many of these sites were present at genes already bound in uninjured podocytes (n = 2839; Fig. 4A and examples in fig. S3A). However, some of these sites were found at 1245 genes not bound in control or D14 (Fig. 4B and examples in fig. S3B). Thus, at D9, WT1 both bound additional sites at already known target genes and acquired new target genes (Fig. 4B). Similar to D14 *mTmG-Nphs2cre* mice, proteinuric BALB/cJ mice also lost many WT1 binding sites at D7 after ADR (fig. S4A).

Genome-wide promoter regions were overrepresented among WT1 binding sites (fig. S3A). The global distribution of WT1 binding sites did not change during injury in either strain of mice (figs. S4B and S5A). However, the intensity of WT1 binding changed over the course of injury. In *mTmG-Nphs2cre* mice, 93% of differentially bound sites increased at D9, whereas almost all binding sites significantly decreased at D14 (fig. S5B). In BALB/cJ mice, WT1 binding significantly changed [false discovery rate (FDR) < 0.05] for 52% of the sites during injury, and 85% of the differential WT1 binding sites decreased in intensity (fig. S4C). We observed differences in the functional distribution among these sites. Most notably, WT1-bound sites that increased in intensity after injury were primarily found in introns (50%) in *mTmG-Nphs2cre* mice, suggesting that WT1 bound additional intronic enhancer sites during the injury response (fig. S5B). These results demonstrate a process whereby, in the early stages of injury, WT1 acquires new binding sites and increases the intensity of its binding at previously bound sites.

Dynamics of WT1 target gene classes during the injury response

We previously defined two classes of WT1 target genes, based on WT1 binding patterns (*4*): class 1 genes that have a single WT1 binding site at the TSS (TSS ± 1 kbp) and class 2 genes that have multiple binding sites within a 500-kb region of the TSS, including those at the TSS. To these, we add class 3 genes that have multiple WT1 binding sites but not at the TSS, and class 4 genes that have a single binding site not within 1 kb of a TSS (Fig. 4C). Unbound genes are defined as not having a WT1 binding site within 500 kb of the TSS. Comparable to our previous findings, class 1/2 genes had a higher range of expression levels in uninjured podocytes. Classes 3 and 4, while expressed at lower levels than class 1/2 genes, were significantly more highly expressed than unbound genes (Fig. 4D). Thus, WT1 binding is a major determinant of gene expression in podocytes, and binding at the TSS is particularly important.

A large number of genes changed their class designation during the course of injury. Many genes not bound in uninjured podocytes became transiently bound at D9. A small number of genes changed from class 3/4 to class 1/2 at D9 and returned to class 3/4 or unbound at D14 (Fig. 4E). Classes 2 and 3 genes showed the greatest changes in WT1 binding, the majority increasing at D9 and decreasing at D14 (P < 0.001; Fig. 4F and fig. S4E). Furthermore, in both strains of mice, many class 1/2 genes became unbound at D14 (Fig. 4E and fig. S4D). At D14, the number of genes with decreased or lost WT1 binding (defined as either decreased number of binding sites or binding intensity) greatly outnumbered bound genes (Fig. 4, E and F). These analyses emphasize the importance of WT1 binding for the response to injury in podocytes and that generally, TF binding is a highly dynamic process regulating gene expression during the response to cellular injury.

WT1 regulated transcriptional network

Eukaryote TFs generally act combinatorially to determine tissue-specific patterns of gene expression. Therefore, we examined TF motif enrichment near those WT1 binding sites whose intensity significantly increased at D9. This analysis highlighted that motifs predicting Forkhead box (FOX), LIM homeobox transcription factor 1-beta (LMX1B), T cell factor 21 (TCF21), and MAF BZIP Transcription Factor B (MAFB) as TFs were potentially cobinding with WT1 (Fig. 4G), all well known to be important in podocytes (*17*–*20*), suggesting that the response to injury involves the basic transcriptional machinery already present in podocytes. TEAD (TEA Domain Transcription Factor 1) sites were also predicted, as were FOS/JUN sites, the former predicting a role for Yes-associated protein-1 (YAP)/Tafazzin (TAZ) in regulating the injury response and the latter suggesting a role for the Activator Protein-1 (AP-1) TF, described to confer protection from glomerulonephritis (*21*). Near WT1 sites uniquely bound at D9, motifs predicting FOX TF cobinding were present, but not other podocyte TFs (Fig. 4H), suggesting that during the injury response, WT1 and FOX TFs may additionally activate a set of enhancers. Motif analysis at sites where WT1 binding was decreased at D14 predicted an entirely different set of TFs, including SP2, Nuclear Respiratory Factor 1 (NRF1), and E2F Transcription Factor 1/4 (E2F1/4) (Fig. 4I). NRF1 and E2F1/4 have been described as repressive TFs (*22*–*24*), suggesting that by D14, a portion of WT1's overall activity may be as part of a repressive complex involved in decreasing the expression of many target genes. Predicted TF motifs at the *Nphs2* and *Synpo* genes are shown in Fig. 3D, adapted from our previous report (*4*).

Functional implications of WT1 dynamic binding

To understand the functional implications of WT1 dynamic binding, we performed RNA-seq analysis on control, D9, and D14 FACS-isolated podocytes from *mTmG-Nphs2-Cre* mice. Gene ontology (GO) analysis based on RNA-seq (Fig. 5A) and ChIP-seq (fig. S6A) datasets was largely consistent with each other in uninjured and D9 podocytes, emphasizing cytoskeletal organization and cell adhesion. Glomerular development was also identified as a GO term at D9, indicating that repair processes involved several genes implicated in the formation of the glomerulus (fig. S6A). Gene expression and binding of WT1 to cytoskeletal and adhesion genes sets were decreased at D14, suggesting that by this point, repair processes in podocytes are greatly diminished (Fig. 5A and fig. S6B). GO analysis of the 1245 genes uniquely bound at D9 (Fig. 4J) was similar to those identified as having increased intensity of WT1 binding at D9 (fig. S6B), indicating that the early response to injury largely involved amplification of the same pathways already operational in uninjured podocytes. Genes represented by GO terms related to RNA stability, nucleotide metabolism, and splicing process showed decreased WT1 binding at D14 (fig. S6B), although their expression levels increased

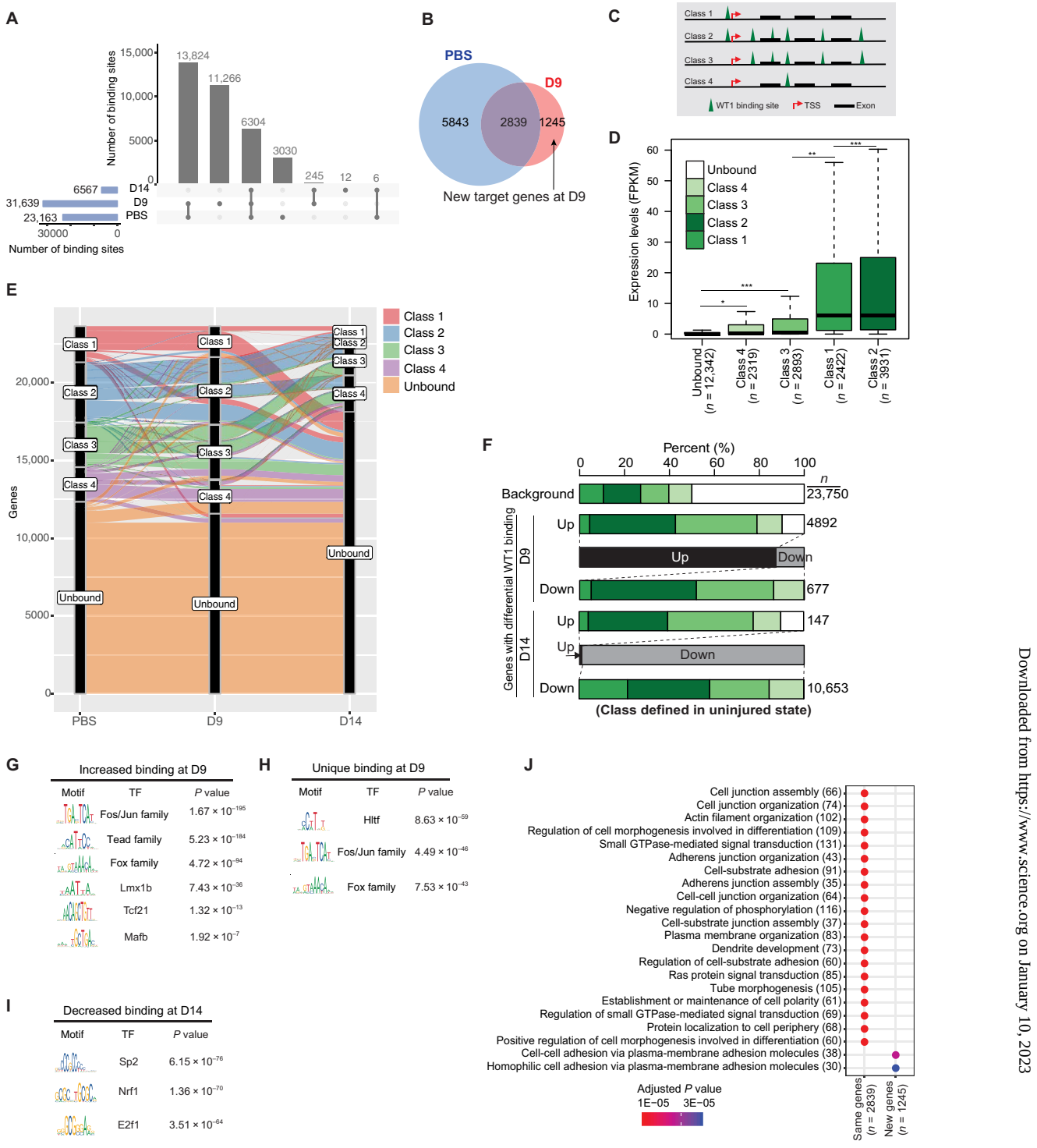

Fig. 4. Dynamics of WT1 binding during the injury response in *mTmG-Nphs2cre* mice. (**A**) Genomic WT1 binding sites at time points. Blue bars: sites per time point. Gray bars: sites common or unique. (**B**) WT1-bound genes: pink, number identified by unique D9 sites; blue, number bound in control; pink only, uniquely bound at D9; blue only, only bound in control. FPKM, fragments per kilobase of transcript per million mapped reads. (**C**) Target gene classes: class 1, single WT1 peak at promoter (±1 kb of TSS); class 2, >1 peak, ±500 kb of promoter; class 3, >1 peak, not at promoter; class 4, single peak, not at promoter. (**D**) Expression of target gene class in isolated podocytes. *P* values: Student's *t* test. ***$P < 0.001$, **$P < 0.01$, and *$P < 0.05$. Box, middle two quartiles; black line, median expression level. (**E**) Gene class changes during injury: class 1 (pink), class 2 (blue), class 3 (green), class 4 (purple), and unbound (orange). *Y* axis, number of genes. (**F**) Proportion of class with differential WT1 binding intensity at D9 or D14 based on class in control, total gene number represented at right of bar. Background: distribution of gene classes in control. (**G**) TF motifs near sites of increased WT1 binding, D9 versus control. (**H**) TF motifs near D9 unique WT1 binding sites. (**I**) TF motifs near sites where WT1 binding decreased at D14 versus control. (**J**) Gene ontology (GO) terms for D9 unique WT1 binding. New genes: GO terms for 1245 genes in (B). Same genes: GO terms for 2839 genes in (B).

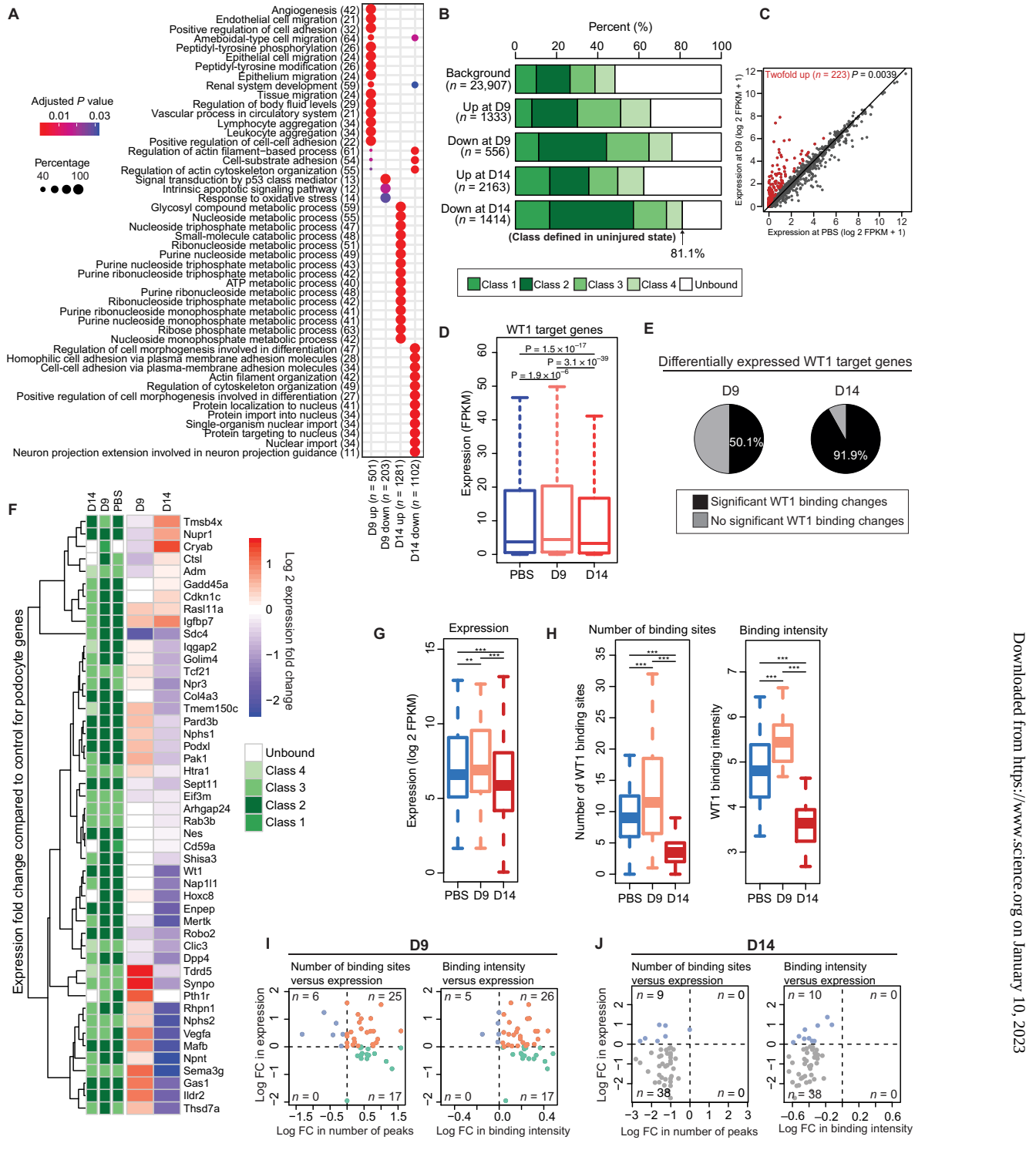

Fig. 5. Transient increase of gene expression during ADR-induced injury in *mTmG-Nphs2cre* mice. (**A**) GO terms enriched for differentially expressed genes (see Methods). Red/blue shading, *P* value; circle size, percent of gene set expressed. (**B**) Class proportions of differentially expressed, as in Fig. 4, using relaxed thresholds (see Methods for statistical analyses). (**C**) D9 versus control expression for D9 uniquely bound genes (red dots, 223 genes with more than twofold change, $P = 0.0039$). (**D**) Expression ranges of WT1 target genes during the course of injury. (**E**) Percentage of differentially expressed genes with significant WT1 binding change. (**F** to **J**) Heatmap showing expression changes and WT1 gene classes for podocyte specific genes. Analysis of podocyte gene set (see text). (G) Expression range, $^{**}P < 0.01$ and $^{***}P < 0.001$. (H) WT1 binding site number (left) and peak intensity (right plot) during the course of injury. (I and J) Correlation plots for (I) D9 and (J) D14. Each dot represents a gene. Left: expression versus binding site number. Right: expression versus binding intensity. FC, fold change. Orange, both increased expression and binding site number; green, decreased expression and increased binding site number; blue, increased expression and decreased peak intensity; gray, both decreased expression and peak intensity.

(Fig. 5A), further suggesting a potential repressive function for WT1 [examples of genes are in fig. S6 (C and D)]. In BALB/cJ mice, GO analysis of genes at which binding increased after injury included regulation of protein processes, while genes at which WT1 binding decreased after injury included paraxial mesodermal development, a set that includes *Foxc2* and *Tead1* (fig. S4, F and G).

WT1 target gene expression changes during injury

WT1-bound genes were found both among those that showed increased and decreased expression levels, further demonstrating that WT1 is an important determinant of gene expression in podocytes. This was the case at both D9 and D14 (Fig. 5B). Classes 2 and 3 genes also showed the greatest overall differences in expression levels between control and D9 or D14 (Fig. 5B). Thus, having multiple WT1 binding sites confers a greater likelihood of gene expression levels changing during the injury process.

Of the 1245 genes uniquely bound by WT1 at D9 (Fig. 4B), 223 increased their expression by at least twofold (Fig. 5C and fig. S5C), and 68 became expressed at D9. Thus, the majority of genes uniquely bound at D9 did not show significant differential expression between control and D9 or D14, demonstrating that changes in expression are more complex than simply reflecting de novo or changes in WT1 binding. Examining the entire set of WT1-bound genes, there was a slight increase in transcript levels, indicating that many WT1-bound genes are not overexpressed during the response to injury (Fig. 5D). Overall, 38 and 64% of differentially expressed genes showed a change in WT1 binding intensity at D9 and D14, respectively (fig. S5D). However, 50% of WT1-bound genes, whose expression significantly changed at D9, also showed a change in the pattern of WT1 binding. At D14, over 90% of WT1-bound genes whose expression changed showed a change in WT1 binding intensity (Fig. 5E), emphasizing the importance of WT1 binding for gene expression during injury.

Transient increase of podocyte-specific gene expression during ADR-induced injury

Transcriptomic data were used to analyze WT1 binding and the expression profile of a recently described podocyte-identifying gene set (*11*) during injury. Most members of this set were class 2 genes. While some class 2 genes remained in the same class, several others converted to class 3 or were unbound by D14 (Fig. 5F). Expression of this gene set significantly increased at D9 ($P < 0.01$) and significantly decreased at D14 ($P < 0.001$; Fig. 5G), as did the average intensity and the number of WT1 peaks (Fig. 5H). While the majority of genes acquired additional WT1-bound sites at D9, several of these genes actually decreased their expression level (Fig. 5I), again indicating that increased number of WT1-bound sites by itself does not necessarily confer increased expression. However, by D14, we observed a stronger correlation between the changes in number of WT1 peaks and expression levels (Fig. 5J). Similar observations were made for the correlation between WT1 binding intensity and expression (Fig. 5, I and J).

WT1 binds at genes encoding other major TFs found in podocytes, including FOXC2, LMX1B, TCF21, and MAFB (*4*); the intensity of WT1 binding at most sites greatly decreases by D14 (fig. S7, A and B). On the basis of RNA-seq analysis, *Wt1*, *Klf6*, *Tcf21*, *Zhx2*, and *Mafb* are the most highly expressed TFs in podocytes, with *Tead1*, *Lmx1b*, and *Foxc2* expressed at lower levels. Most of these TFs' expressions increased at D9 and decreased at D14, indicating that the major transcriptional network in podocytes transiently increased during the injury process (fig. S7C). It is likely that the concerted action of several of these TFs accounts for maximal expression of *Nphs2* and *Synpo* during the process of podocyte injury.

DISCUSSION

Previous studies have identified WT1 target genes sets in podocytes and nephron progenitor cells (*3*, *4*, *25*). In podocytes, WT1 targets most familial nephrotic syndrome and FSGS genes (table S4) (*4*). In addition, among nearly 900 recently identified expression Quantitative Trait Loci (eQTLs) for human nephrotic syndrome (*26*), 318 were within 10 kb of a WT1 binding site where binding changed during the response to injury (104 eQTLs that showed both increased WT1 binding at D9 and decreased binding at D14 are listed in table S5, with change in class genes after ADR injury). Here, we studied how WT1 regulates gene expression during the course of ADR-induced injury in both murine and human podocytes. Our study validates human kidney organoids as a model for podocyte injury. In *mTmG-Nphs2cre* mice, WT1 DNA binding and expression of many genes important to maintaining podocyte integrity transiently increased at the onset of proteinuria, before decreasing at later stages of podocyte injury. However, among the entire set of WT1 target genes, both increased and decreased expression levels were observed upon changes in WT1 binding, suggesting that WT1 may have both activator and repressor functions. Genes whose expression changed during the course of injury were related to multiple pathways known to be important in podocytes, including extracellular matrix genes and their integrin receptors, glomerular slit diaphragm proteins, and actin regulatory proteins. Potential binding sites for several other TFs important in podocytes were found near WT1-bound sites. In addition, at two important target genes, *Nphs2* and *Synpo*, ADR injury resulted in the transition from open to closed chromatin state at these genes, correlating with the loss of WT1 binding and gene expression, establishing WT1 as a major regulator of gene expression in response to podocyte injury. Our analysis also indicates that when multiple enhancers drive expression of a specific target gene, even in an individual cell lineage, these enhancers may be bound by distinct groupings of TFs. This suggests that levels of gene expression reflect the integration of multiple enhancers, each of which might contribute differently to gene expression.

Podocytes have one of the most complex cell morphologies among metazoan organisms, most obvious in the elaboration of FPs that are essential for maintaining the GFB. The cytoskeletal assembly mechanisms that form, maintain, and repair FPs have only recently begun to be understood (*27*). Complex cytoskeletal assembly requires the conserved action of many actin binding and regulatory proteins, many of which are WT1 target genes. For a large number of these genes, WT1 binding and their expression levels were increased at D9. It is not known whether foot process morphology results from a particular combination of cytoskeletal and adhesion proteins found in podocytes, such as specific combinations of Rho guanosine triphosphatase activating proteins and guanine nucleotide exchange factors. If this is found to be the case, then WT1, acting with other TFs, may provide the specificity in determining the set of cytoskeletal regulatory proteins expressed in normal podocytes and amplified in response to injury. Integrin receptors for the extracellular matrix are also integrally involved in determining cell morphology.

In contrast to cytoskeleton and adhesion-related genes, many genes involved in energy metabolism were found to have decreased expression levels particularly at D14. Mitochondrial damage has been shown to be a major contributor to ADR-induced podocyte damage (*28*, *29*). WT1 also binds several genes encoding components that regulate the tricarboxylic acid cycle and adenosine 5′-triphosphate production in mitochondria. In many cases, WT1 binding was inversely correlated with gene expression, suggesting that in addition to serving as a transcriptional activator, WT1 may, for distinct gene sets, act in a repressor complex. Such a function has previously been demonstrated for WT1 (*30*, *31*); however, it is not known what determines an activator versus repressor function for WT1.

On the basis of our results, we suggest a model whereby WT1, along with cofactors, activates a set of TFs that may form a complex to regulate the transcription of specific podocyte genes. In injured podocytes, an early response occurs, defined by an increase in WT1 DNA binding that may recruit additional enhancer elements that loop into the TSS, increase activating epigenetic marks in the vicinity of the TSS, and recruit additional coactivators to increase transcription at target genes (summarized in Fig. 6). This leads to an open chromatin conformation, resulting in an increase of gene expression crucial to maintain podocytes function. This attempt at repair is followed by decreased expression of WT1 that, in turn, results in a decrease in its binding to TF target genes. Consequently, there is a decrease in expression of genes required to maintain the filtration barrier, resulting in foot process effacement and proteinuria. Therefore, understanding the epigenetic landscape that occurs during podocyte injury could help identify the key epigenetic changes that lead to FSGS. These epigenetic hallmarks may serve as biomarkers of FSGS diagnosis and progression and facilitate the development of previously unrecognized therapeutic approaches targeting the epigenome. An additional point related to enhancer usage emerges from this study that may be generalizable to TF biology in general and particularly in response to disease. WT1 binding at distinct enhancers and promoters does not simply reflect the overall level of WT1 but may differ between individual binding sites. Recent studies have demonstrated redundancy among multiple enhancers affecting expression of individual genes during development (*32*). In contrast, our results suggest that enhancers may make distinct contributions to gene expression during the response to injury.

The cellular response to injury in human disease is complex. Some immediate responses, such as those that trigger secretion or changes in cell morphology, may not involve changes in gene expression. However, any process that is maintained over hours to days or longer likely involves transcriptional reprogramming to respond to the injury. As documented in our report, the response to injury in podocytes appears to involve the WT1 TF programming, a process aimed at repairing the damage and restoring normal cell function. These results suggest a paradigm whereby tissue-specific TFs are instrumental in driving responses to cellular injury.

METHODS

Cell culture

Immortalized mouse podocytes were cultured with RPMI 1640 medium (Corning) with 10% fetal bovine serum, 5% sodium pyruvate solution (100 mM; Thermo Fisher Scientific). Undifferentiated cells were cultured at 33°C in the presence of murine interferon-γ (10 U/ml; IFN-γ) (R&D systems). To induce podocyte, differentiation cells were shifted to 37°C for 14 days in the absence of IFN-γ.

Mice

All animal studies were carried out in accordance with the guidelines of the Institutional Animal Care and Use Committee at Boston

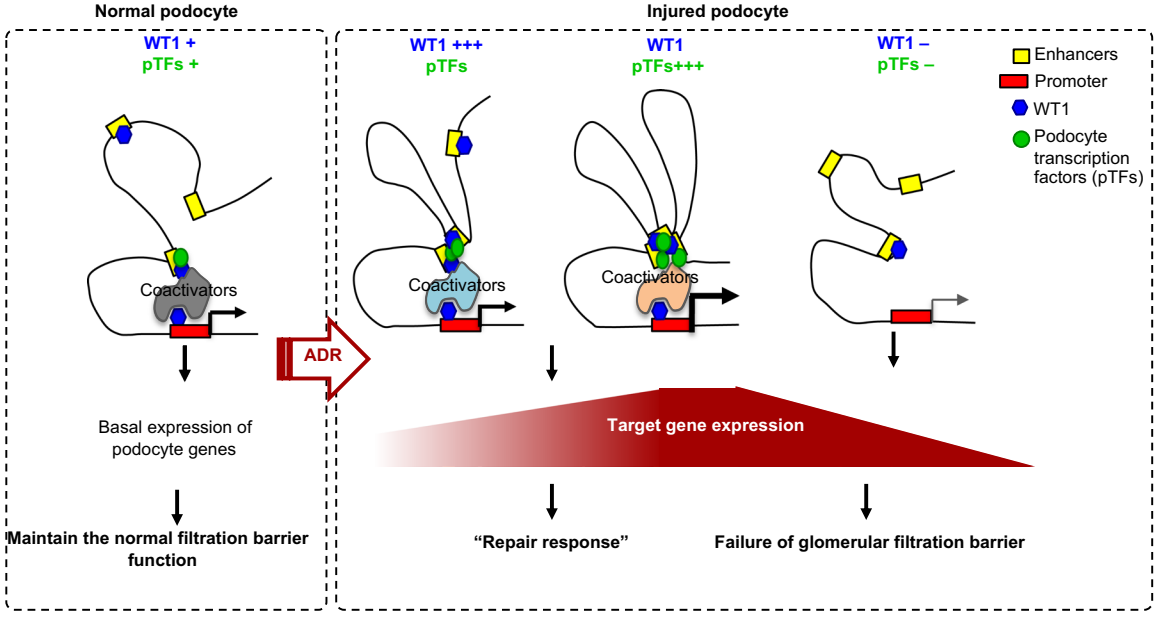

Fig. 6. Model of WT1 transcriptional reprogramming during podocyte injury. In normal podocytes, WT1 recruits a set of TFs that forms a complex to regulate the transcription of specific podocyte genes. In injured podocytes, an early response occurs by an increase in WT1 DNA binding that increases the recruitment of epigenetic coactivators. This leads to open chromatin at additional enhancers followed by increased DNA binding of additional podocyte TFs and increased transcription of podocyte-specific genes. This repair response is followed by the decreased expression of WT1 and decreased binding of WT1 and other TFs to target genes and the inability to maintain the filtration barrier.

Children's Hospital. BALB/cJ mice were purchased from the Jackson laboratory. *mT/mG-Nphs2cre* mice were obtained by breeding *R26-mTmG* mice (the Jackson laboratory, 007676) with *Nphs2cre* mice expressing red fluorescence before Cre recombination and green fluorescence after recombination in podocytes (*33*). This system was used to isolate podocytes by flow cytometry (FACS). BALB/cJ and *mT/mG-Nphs2cre* mice were injected with ADR (10.5 and 18 mg/kg, respectively; Cayman Chemical) or PBS control, through the retro-orbital venous sinus under isoflurane anesthesia. *mT/mG-Nphs2cre* mice received two injections at a 1-week interval. Kidneys were harvested at D3, D5, and D7 for BALB/cJ mice and at D5, D7, D9, D10, and D14 for *mT/mG-Nphs2cre* mice. $WT1^{flox/flox}$/*Nphs2-CreERT2/TdTomato* mice (WT1 CKO) were obtained by breeding $WT1^{flox/+}$ mice (*34*) with *Nphs2-CreERT2*, a tamoxifen-inducible improved Cre recombinase (CreERT2) under the regulation of *Nphs2* (podocin) gene promoter (*12*), and with *R26R-tdTomato* mice (the Jackson laboratory 007909). This system was used to isolate tdTomato-expressing podocytes. $WT1^{flox/flox}$/*Nphs2-CreERT2/TdTomato* mice were given tamoxifen (120 mg/kg) during three consecutive days by intraperitoneal injections. Kidneys were harvested 2 weeks after the first injection. Genotyping primers are given in table S1.

Glomerular preparation and podocytes isolation

Glomerular preparation and isolation of GFP-positive (GFP^+) podocytes from 6- to 8-week-old *mT/mG-Nphs2cre* and $WT1^{flox/flox}$/*icre/Tdtomato* mice were done, as described previously (*4*). Renal arteries were perfused with Dynabeads M-450 in Hank's balanced salt solution (HBSS), and dissected kidneys were minced and incubated in digestion solution for 15 min at 37°C [collagenase II (300 U/ml; Worthington), pronase E (1 mg/ml; Sigma-Aldrich), and deoxyribonuclease I (50 U/μl; AppliChem) in HBSS]. The digest was passed through 100-μm sieves twice, washed with HBSS, and spun down, and glomeruli were isolated using a magnetic concentrator. Glomeruli were dissociated into a single-cell suspension by incubation in digestion solution at 37°C on an incubator shaker for 40 min. Cells were sieved through a 40-μm filter, and GFP^+ cells were FACS sorted on a FACS MoFlo flow cytometer.

Kidney organoid generation and ADR treatment

H9 hESCs were differentiated into kidney organoids, as reported previously (*35*, *36*). Briefly, hESCs were differentiated into metanephric mesenchyme (MM) cells by a three-step directed differentiation protocol. MM cells were resuspended in 96-well, round-bottom, ultralow-attachment plates (Corning), and further differentiation was promoted by Fibroblast Growth Factor-9 (FGF9) (R&D systems) and transient treatment of CHIR (Tocris). After day 21 of differentiation, organoids were cultured in basic differentiation medium consisting of Advanced RPMI 1640 and L-GlutaMax (Life Technologies) until day 49 of differentiation. Then, kidney organoids were treated with 10 μM ADR for 24 hours from day 49 of differentiation. Organoids were harvested after 1, 4, 7, and 10 days of ADR injury (on day 50, 53, 56, and 59 of differentiation). Human organoid and stem cell experiments were approved by the Partners Institutional Biosafety Committee, and Partners Human Embryonic Stem Cell Research Oversight Committee.

Western blot

Whole-cell lysates were from immortalized mouse podocytes; isolated podocytes and organoids were prepared in high-salt radioimmunoprecipitation assay [500 mM NaCl, 50 mM tris-HCl (pH 7.4), 5 mM EDTA, 1 mM EGTA, 0.1% SDS, 1% Igepal, 0.5% sodium deoxycholate, and 1× Roche protease inhibitor mix]. Samples were subjected to 8% SDS–polyacrylamide gel electrophoresis and transferred to nitrocellulose membrane. Standard Western blotting was performed with antibodies against WT1 (Santa Cruz Biotechnology, sc-192), glyceraldehyde-3-phosphate dehydrogenase (Sigma-Aldrich), Synpo (gift from P. Mundel), and podocin (P35 antibody, gift from C. Antignac).

Immunofluorescence

Kidney sections were fixed by 4% paraformaldehyde (PFA) for 5 min and immunostained with antibodies against WT1 (Santa Cruz Biotechnology, sc-192) and counterstained with 4′,6-diamidino-2-phenylindole (DAPI). A 4% PFA–fixed kidney organoids were incubated in blocking buffer (0.3% Triton X-100 and 5% normal donkey or goat serum) for 1 hour at room temperature and then washed three times in PBS. The organoids were incubated with primary antibodies against WT1 (1:100; Santa Cruz Biotechnology, sc-192), podocalyxin (1:500; AF1658, R&D Systems), Synpo (1:200; gift from P. Mundel), and Nphs1 (1:200; GP-N2, Progen) in antibody dilution buffer (0.3% Triton X-100 and 1% bovine serum albumin in PBS) for 3 hours at room temperature. The organoids were then washed three times with PBS. The organoids were incubated with secondary antibodies in antibody dilution buffer for 1 hour at room temperature and then washed with PBS three times for 30 min each and counterstained with DAPI.

RNA extraction, complementary DNA, and RT-qPCR analysis

Total RNA from immortalized mouse podocytes, isolated podocytes, and organoids was extracted using TRIzol Reagent (Invitrogen). Oligo(dT)-primed complementary DNAs were synthesized from total RNAs using Superscript III reverse transcriptase (Invitrogen) and amplified by polymerase chain reaction (PCR) using the following thermal cycling program: 95°C for 5 min, 40 cycles of 5 s at 95°C, 5 s at 60°C, and 10 s at 72°C, followed by a 5-min extension time at 72°C. All data were normalized to *Gapdh* using the $\Delta\Delta C_t$ method. Primers used are described in table S2. Experiments were performed by triplicate.

ChIP-qPCR and ChIP-seq

Chromatin from isolated glomeruli and isolated podocytes was prepared from 7- to 8-week-old BALB/cJ, *mT/mG-Nphs2cre*, and $WT1^{flox/flox}$/*Nphs2iCRE* mice. For WT1 ChIP assays, chromatin was immunoprecipitated from either isolated glomeruli from two kidneys or 10 million immortalized mouse podocytes (four independent experiments were performed per condition for BALB/cJ mice and three independent experiments for *mT/mG-Nphs2cre* mice and immortalized mouse podocytes). For histone ChIP assays, we immunoprecipitated chromatin from FACS-isolated podocytes from 10 mice, or 10^6 of immortalized mouse podocytes were used per immunoprecipitation (three independent experiments were performed per condition for *mT/mG-Nphs2cre* mice and immortalized mouse podocytes). Samples were fixed with 1% formaldehyde in PBS for 5 min at room temperature before termination with 0.125 M glycine. Cells were then lysed in sonication buffer, as described previously (*4*). Cross-linked chromatin was sonicated to obtain DNA fragments of 200 to 600 bp. Immunoprecipitations were performed, as described previously. Antibodies used were as follows: WT1 (Santa Cruz Biotechnology, sc-192), H3K9me3 (07-523, Millipore), H3K27ac (39135,

Active Motif), H3K27me3 (C15410195, Diagenode), H3K4me3 (07-473, Millipore), H3K4me1 (07-436, Millipore), H4K8ac (07-328, Millipore), and H4K12ac (04-119, Millipore). DNA was recovered by phenol-chloroform extraction and ethanol precipitation. Reverse transcription quantitative PCR (RT-qPCR) analyses were performed on immunoprecipitated DNA using specific primers described in table S3. Fold enrichment of ChIP versus immunoglobulin G (IgG) control was calculated as $2((C_t(\text{IgG}) - C_t(\text{input})) - (C_t(\text{ChIP}) - C_t(\text{input})))$.

Library preparation ChIP-seq

ChIP-seq libraries were prepared using NEBNext DNA library preparation reagents (E6040) and the protocol and reagents concentrations described in the Illumina Multiplex ChIP-seq DNA sample Prep Kit. Libraries were indexed using a single indexed PCR primer. Libraries were quantified by Qubit (Invitrogen) and sequenced using a HiSeq 2000 (Illumina) to generate 50-bp single-end reads.

Library preparation RNA-seq

Total RNA extracted from GFP^+ podocytes was quantified on the Qubit RNA assay (Invitrogen). RNA quality was checked using Agilent Bioanalyzer 2100 RNA Nano chip (Agilent). RNA samples exceeding an RNA integrity number of 8 were submitted to sequencing. Five micrograms of RNA was used as a starting material for ribosomal RNA (rRNA) depletion using the Ribo-Zero Magnetic Gold Kit (human/mouse/rat; Epicentre). rRNA-depleted samples were analyzed on an Agilent Bioanalyzer to ensure that the majority of rRNA was depleted before the library was prepared. A total of 100 ng of rRNA-depleted RNA was then used in the NEBNext Ultra Directional RNA-seq Kit (E7420L) to generate sequencing libraries according to the manufacturer's instructions.

Statistics

Two-tailed paired Student's *t* test was used to determine statistical significance between PBS and ADR conditions. Bars represent means and error bars ± SEMs. $^{***}P < 0.001$, $^{**}P < 0.01$, and $^{*}P < 0.05$. Analysis of variance (ANOVA) with Tukey's multiple comparisons test was used to compare different time points for WT1 ChIP-qPCR and histone ChIP-qPCR ($^{****}P < 0.0001$, $^{***}P < 0.001$, $^{**}P < 0.01$, and $^{*}P < 0.05$). Multiple *t* tests with FDR determined using the two-stage linear step-up procedure of Benjamini, Krieger, and Yekutieli were used to compare different conditions (PBS/ADR and control/WT1 CKO) for histone ChIP-qPCR. *P* values for analyses in Fig. 5 were assigned using a one-sided paired Wilcoxon test.

Bioinformatic analysis

Alignments

For ChIP-seq samples, reads after removing adaptor sequences were mapped to mm9 using Bowtie1 (*37*), with the unique mapping option. For RNA-seq, Bowtie1 (*37*) and Tophat2 (*38*) were used, with the no novel junction option.

Genomic annotations

The genomic annotations for promoters (with 500-bp margins), exons, 5′ untranslated region (5′UTR), 3′UTR, and genic regions were obtained from the University of California, Santa Cruz (UCSC) genome browser (mm9, RefSeq).

ChIP-seq profile normalization

Although we did not have a spike-in sample in our experiments, we checked that no further normalization was necessary by computational analysis. We estimated the background noise level in the ChIP-seq profile using the approach we described previously (*39*). The basic idea is that the background "noise" levels should be similar under different experimental conditions, independent of binding intensity, for the profiles to be directly compared. We estimated the background noise levels by calculating the median absolute deviation of signal differences of adjacent bins; this quantity measures how much the profile fluctuates, while being robust to the actual signal in the data. When we applied this method to the ChIP-seq signals in PBS, ADR D9, and ADR D14, we found that the noise levels are fairly consistent across conditions, with only up to 3% difference.

Peak detection for WT1 ChIP-seq

Only uniquely aligned reads were used for downstream analysis of ChIP-seq samples. After checking the reproducibility between replicates, reads in replicates were combined. Statistically significant peaks were detected using MACS2 callpeak function with a *q* value of 0.05 (*40*).

Differential bindings of WT1

Starting with the union of peaks from two conditions, read counts were obtained and compared between two conditions using Diffbind R package (*41*). This package uses Deseq2 (*42*) to assess the dispersion and significance of the fold changes. The WT1 changes with FDR < 0.05 and a fold change of >1.4 were considered significant.

TF enrichment around WT1 peaks

For the significantly increased WT1 bindings at ADR D9 compared to PBS (FDR < 0.05 and a fold change of >2), DNA sequences were obtained with a 200-bp window (Fig. 4G). For the control sequences, the same number of WT1 binding sites was chosen from the locations where WT1 binding does not change significantly at D9 (*P* value of >0.05 and a fold change of <1.4). The enrichment of TF motifs was compared between the two groups using the Multiple Expression motifs for Motif Elicitation (MEME) suite Analysis of Motif Enrichment (AME) (*43*) with default parameters. TF motif sequences were collected from the JASPAR CORE 2018 vertebrate database (*44*) and Jolma *et al.* (*45*). Among the significantly enriched TFs, those that are silent or low expressed in podocytes were filtered. The same procedure was done for the prediction of enriched TFs at the significantly decreased WT1 binding sites at D14 (Fig. 4I). For the prediction of enriched TFs for unique WT1 peaks at D9, DNA sequences were obtained with a 200-bp window from D9-unique WT1 peak summits. Persistent peak sites found in PBS, D9, and D14 were used as control sites (Fig. 4H).

TF binding prediction near WT1 binding sites for Nphs2 and Synpo

For the WT1 binding sites overlapping with regions of high conservation scores, the locations of key TFs in podocytes such as TEAD1, FOXC2, TCF21, WT1, MAFB, and LMX1B and several TFs enriched for differential WT1 binding sites during the course of ADR injury were predicted using the MEME suite Find Individual Motif Occurrences (FIMO) with $P = 0.01$ (*46*). A window size of 100 bp was used from the WT1 peak summits to extract DNA sequences.

Association between WT1 peaks and genes

To infer potential target genes of WT1 peaks, we determined whether a binding site is in the proximal region of a gene, defined as 5 kb upstream and 1 kb downstream from TSSs, or in the distal region, defined as 500 kb from TSS. If so, then we consider that gene (or genes) to be associated with the WT1 binding site. For the de novo WT1 peaks at D9, we used a more stringent criteria of 10 kb upstream and downstream from TSSs (Fig. 4). For the analysis of expression

changes for WT1 target genes in Fig. 5D, a 10-kb margin was used to associate potential targets of WT1 bindings.

Gene classes based on WT1 binding

For each condition, gene classes were defined as in Kann *et al.* (*4*) and further modified. Specifically, class 1 includes those genes whose promoters (±1 kb from TSSs) are bound by a single WT1 peak within the 500-kb region of the TSS. Class 2 includes those genes with multiple WT1 bindings, including peaks at the promoter. Class 3 includes those genes having multiple WT1 bindings except at the promoter. Class 4 includes those genes having a single peak in a non-promoter region within the 500-kb region of TSS.

Expression quantification

To quantify expression levels, Cufflinks (*47*) was used with default parameters. The transcriptional annotations from UCSC mm9 were used. The fragments per kilobase of transcript per million mapped reads values were calculated for each gene.

Differentially expressed genes

Three different methods—Cuffdiff (*47*), Deseq2 (*42*), and EdgeR (*48*)—were used to identify genes with significant expression changes between conditions for the stringent gene set in Fig. 5A. A q value of 0.05 was used for Cuffdiff as a threshold; a P value of 0.05 was used for Deseq2 and EdgeR. The genes detected from at least two methods were used for the GO analysis. For Fig. 5B, differentially expressed genes were determined by relaxed criteria, with a P value of 0.05 from Cuffdiff.

GO analysis

For the significantly changed WT1 binding sites, GREAT version 3 (*49*) was used to determine GO terms associated with the WT1 binding sites, with default parameters. For the genes with significant expression changes, DAVID (*50*) was used. The results were visualized using R package clusterProfiler (*51*).

SUPPLEMETARY MATERIALS

Supplementary material for this article is available at http://advances.sciencemag.org/cgi/content/full/6/30/eabb5460/DC1

View/request a protocol for this paper from *Bio-protocol*.

REFERENCES AND NOTES

1. R. C. Wiggins, The spectrum of podocytopathies: A unifying view of glomerular diseases. *Kidney Int.* **71**, 1205–1214 (2007).
2. V. D'Agati, Pathologic classification of focal segmental glomerulosclerosis. *Semin. Nephrol.* **23**, 117–134 (2003).
3. L. Dong, S. Pietsch, C. Englert, Towards an understanding of kidney diseases associated with WT1 mutations. *Kidney Int.* **88**, 684–690 (2015).
4. M. Kann, S. Ettou, Y. L. Jung, M. O. Lenz, M. E. Taglienti, P. J. Park, B. Schermer, T. Benzing, J. A. Kreidberg, Genome-wide analysis of Wilms' tumor 1-controlled gene expression in podocytes reveals key regulatory mechanisms. *J. Am. Soc. Nephrol.* **26**, 2097–2104 (2015).
5. J. A. Kreidberg, H. Sariola, J. M. Loring, M. Maeda, J. Pelletier, D. Housman, R. Jaenisch, WT-1 is required for early kidney development. *Cell* **74**, 679–691 (1993).
6. M. S. Orloff, S. K. Iyengar, C. A. Winkler, K. A. Goddard, R. A. Dart, T. S. Ahuja, M. Mokrzycki, W. A. Briggs, S. M. Korbet, P. L. Kimmel, E. E. Simon, H. Trachtman, D. Vlahov, D. M. Michel, J. S. Berns, M. C. Smith, J. R. Schelling, J. R. Sedor, J. B. Kopp, Variants in the Wilms' tumor gene are associated with focal segmental glomerulosclerosis in the African American population. *Physiol. Genomics* **21**, 212–221 (2005).
7. P. Thorner, M. McGraw, S. Weitzman, J. W. Balfe, M. Klein, R. Baumal, Wilms' tumor and glomerular disease. Occurrence with features of membranoproliferative glomerulonephritis and secondary focal, segmental glomerulosclerosis. *Arch. Pathol. Lab. Med.* **108**, 141–146 (1984).
8. S. Ito, A. Takata, H. Hataya, M. Ikeda, H. Kikuchi, J. Hata, M. Honda, Isolated diffuse mesangial sclerosis and Wilms tumor suppressor gene. *J. Pediatr.* **138**, 425–427 (2001).
9. A. Binczak-Kuleta, J. Rubik, M. Litwin, M. Ryder, K. Lewandowska, O. Taryma-Lesniak, J. S. Clark, R. Grenda, A. Ciechanowicz, Retrospective mutational analysis of NPHS1, NPHS2, WT1 and LAMB2 in children with steroid-resistant focal segmental glomerulosclerosis - a single-centre experience. *Bosn. J. Basic Med. Sci.* **14**, 89–93 (2014).
10. K. Iijima, T. Someya, S. Ito, K. Nozu, K. Nakanishi, K. Matsuoka, H. Ohashi, M. Nagata, K. Kamei, S. Sasaki, Focal segmental glomerulosclerosis in patients with complete deletion of one WT1 allele. *Pediatrics* **129**, e1621–e1625 (2012).
11. N. Karaiskos, M. Rahmatollahi, A. Boltengagen, H. Liu, M. Hoehne, M. Rinschen, B. Schermer, T. Benzing, N. Rajewsky, C. Kocks, M. Kann, R.-U. Muller, A single-cell transcriptome atlas of the mouse glomerulus. *J. Am. Soc. Nephrol.* **29**, 2060–2068 (2018).
12. H. Yokoi, M. Kasahara, M. Mukoyama, K. Mori, K. Kuwahara, J. Fujikura, Y. Arai, Y. Saito, Y. Ogawa, T. Kuwabara, A. Sugawara, K. Nakao, Podocyte-specific expression of tamoxifen-inducible Cre recombinase in mice. *Nephrol. Dial. Transplant.* **25**, 2120–2124 (2010).
13. A. J. Bannister, T. Kouzarides, Regulation of chromatin by histone modifications. *Cell Res.* **21**, 381–395 (2011).
14. Y. Wang, Y. P. Wang, Y. C. Tay, D. C. Harris, Progressive adriamycin nephropathy in mice: Sequence of histologic and immunohistochemical events. *Kidney Int.* **58**, 1797–1804 (2000).
15. N. Papeta, Z. Zheng, E. A. Schon, S. Brosel, M. M. Altintas, S. H. Nasr, J. Reiser, V. D. D'Agati, A. G. Gharavi, Prkdc participates in mitochondrial genome maintenance and prevents Adriamycin-induced nephropathy in mice. *J. Clin. Invest.* **120**, 4055–4064 (2010).
16. J.-K. Guo, A. L. Menke, M.-C. Gubler, A. R. Clarke, D. Harrison, A. Hammes, N. D. Hastie, A. Schedl, WT1 is a key regulator of podocyte function: Reduced expression levels cause crescentic glomerulonephritis and mesangial sclerosis. *Hum. Mol. Genet.* **11**, 651–659 (2002).
17. T. Burghardt, J. Kastner, H. Suleiman, E. Rivera-Milla, N. Stepanova, C. Lottaz, M. Kubitza, C. A. Boger, S. Schmidt, M. Gorski, U. de Vries, H. Schmidt, I. Hertting, J. Kopp, A. Rascle, M. Moser, I. M. Heid, R. Warth, R. Spang, J. Wegener, C. T. Mierke, C. Englert, R. Witzgall, LMX1B is essential for the maintenance of differentiated podocytes in adult kidneys. *J. Am. Soc. Nephrol.* **24**, 1830–1848 (2013).
18. B. He, L. Ebarasi, Z. Zhao, J. Guo, J. R. Ojala, K. Hultenby, S. De Val, C. Betsholtz, K. Tryggvason, Lmx1b and FoxC combinatorially regulate podocin expression in podocytes. *J. Am. Soc. Nephrol.* **25**, 2764–2777 (2014).
19. N. Morito, K. Yoh, M. Ojima, M. Okamura, M. Nakamura, M. Hamada, H. Shimohata, T. Moriguchi, K. Yamagata, S. Takahashi, Overexpression of Mafb in podocytes protects against diabetic nephropathy. *J. Am. Soc. Nephrol.* **25**, 2546–2557 (2014).
20. D. Nilsson, M. Heglind, Z. Arani, S. Enerback, Foxc2 is essential for podocyte function. *Physiol. Rep.* **7**, e14083 (2019).
21. H. T. Cook, R. Tarzi, Z. D'Souza, G. Laurent, W. C. Lin, T. J. Aitman, F. Mechta-Grigoriou, J. Behmoaras, AP-1 transcription factor JunD confers protection from accelerated nephrotoxic nephritis and control podocyte-specific Vegfa expression. *Am. J. Pathol.* **179**, 134–140 (2011).
22. J. Hsu, J. Sage, Novel functions for the transcription factor E2F4 in development and disease. *Cell Cycle* **15**, 3183–3190 (2016).
23. D. Phan, C.-J. Cheng, M. Galfione, F. Vakar-Lopez, J. Tunstead, N. E. Thompson, R. R. Burgess, S. M. Najjar, L.-Y. Yu-Lee, S.-H. Lin, Identification of Sp2 as a transcriptional repressor of carcinoembryonic antigen-related cell adhesion molecule 1 in tumorigenesis. *Cancer Res.* **64**, 3072–3078 (2004).
24. T. Tsujita, V. Peirce, L. Baird, Y. Matsuyama, M. Takaku, S. V. Walsh, J. L. Griffin, A. Uruno, M. Yamamoto, J. D. Hayes, Transcription factor Nrf1 negatively regulates the cystine/glutamate transporter and lipid-metabolizing enzymes. *Mol. Cell. Biol.* **34**, 3800–3816 (2014).
25. S. Hartwig, J. Ho, P. Pandey, K. Macisaac, M. Taglienti, M. Xiang, G. Alterovitz, M. Ramoni, E. Fraenkel, J. A. Kreidberg, Genomic characterization of Wilms' tumor suppressor 1 targets in nephron progenitor cells during kidney development. *Development* **137**, 1189–1203 (2010).
26. C. E. Gillies, R. Putler, R. Menon, E. Otto, K. Yasutake, V. Nair, P. Hoover, D. Lieb, S. Li, S. Eddy, D. Fermin, M. T. McNulty; Nephrotic Syndrome Study Network (NEPTUNE), N. Hacohen, K. Kiryluk, M. Kretzler, X. Wen, M. G. Sampson, An eQTL landscape of kidney tissue in human nephrotic syndrome. *Am. J. Hum. Genet.* **103**, 232–244 (2018).
27. E. Torban, F. Braun, N. Wanner, T. Takano, P. R. Goodyer, R. Lennon, P. Ronco, A. V. Cybulsky, T. B. Huber, From podocyte biology to novel cures for glomerular disease. *Kidney Int.* **96**, 850–861 (2019).
28. J. F. O'Toole, Renal manifestations of genetic mitochondrial disease. *Int. J. Nephrol. Renovasc. Dis.* **7**, 57–67 (2014).
29. Q.-J. Wei, H. Xu, N. Guan, Y.-L. Ren, X. Y. Liu, G.-H. Wu, S.-N. Zhu, Overproduction of mitochondrial fission proteins in membranous nephropathy in children. *Kidney Blood Press. Res.* **43**, 1927–1934 (2018).
30. B. Carpenter, K. J. Hill, M. Charalambous, K. J. Wagner, D. Lahiri, D. I. James, J. S. Andersen, V. Schumacher, B. Royer-Pokora, M. Mann, A. Ward, S. G. E. Roberts, BASP1 is a transcriptional cosuppressor for the Wilms' tumor suppressor protein WT1. *Mol. Cell. Biol.* **24**, 537–549 (2004).

31. L. M. Green, K. J. Wagner, H. A. Campbell, K. Addison, S. G. E. Roberts, Dynamic interaction between WT1 and BASP1 in transcriptional regulation during differentiation. *Nucleic Acids Res.* **37**, 431–440 (2009).
32. M. Osterwalder, I. Barozzi, V. Tissières, Y. Fukuda-Yuzawa, B. J. Mannion, S. Y. Afzal, E. A. Lee, Y. Zhu, I. Plajzer-Frick, C. S. Pickle, M. Kato, T. H. Garvin, Q. T. Pham, A. N. Harrington, J. A. Akiyama, V. Afzal, J. Lopez-Rios, D. E. Dickel, A. Visel, L. A. Pennacchio, Enhancer redundancy provides phenotypic robustness in mammalian development. *Nature* **554**, 239–243 (2018).
33. M. D. Muzumdar, B. Tasic, K. Miyamichi, L. Li, L. Luo, A global double-fluorescent Cre reporter mouse. *Genesis* **45**, 593–605 (2007).
34. F. Gao, S. Maiti, N. Alam, Z. Zhang, J. M. Deng, R. R. Behringer, C. Lécureuil, F. Guillou, V. Huff, The Wilms tumor gene, *Wt1*, is required for *Sox9* expression and maintenance of tubular architecture in the developing testis. *Proc. Natl. Acad. Sci. U.S.A.* **103**, 11987–11992 (2006).
35. R. Morizane, J. V. Bonventre, Generation of nephron progenitor cells and kidney organoids from human pluripotent stem cells. *Nat. Protoc.* **12**, 195–207 (2017).
36. R. Morizane, A. Q. Lam, B. S. Freedman, S. Kishi, M. T. Valerius, J. V. Bonventre, Nephron organoids derived from human pluripotent stem cells model kidney development and injury. *Nat. Biotechnol.* **33**, 1193–1200 (2015).
37. B. Langmead, C. Trapnell, M. Pop, S. L. Salzberg, Ultrafast and memory-efficient alignment of short DNA sequences to the human genome. *Genome Biol.* **10**, R25 (2009).
38. D. Kim, G. Pertea, C. Trapnell, H. Pimentel, R. Kelley, S. L. Salzberg, TopHat2: Accurate alignment of transcriptomes in the presence of insertions, deletions and gene fusions. *Genome Biol.* **14**, R36 (2013).
39. S. Peng, A. A. Alekseyenko, E. Larschan, M. I. Kuroda, P. J. Park, Normalization and experimental design for ChIP-chip data. *BMC Bioinformatics* **8**, 219 (2007).
40. Y. Zhang, T. Liu, C. A. Meyer, J. Eeckhoute, D. S. Johnson, B. E. Bernstein, C. Nusbaum, R. M. Myers, M. Brown, W. Li, X. S. Liu, Model-based analysis of ChIP-Seq (MACS). *Genome Biol.* **9**, R137 (2008).
41. C. S. Ross-Innes, R. Stark, A. E. Teschendorff, K. A. Holmes, H. R. Ali, M. J. Dunning, G. D. Brown, O. Gojis, I. O. Ellis, A. R. Green, S. Ali, S. F. Chin, C. Palmieri, C. Caldas, J. S. Carroll, Differential oestrogen receptor binding is associated with clinical outcome in breast cancer. *Nature* **481**, 389–393 (2012).
42. M. I. Love, W. Huber, S. Anders, Moderated estimation of fold change and dispersion for RNA-seq data with DESeq2. *Genome Biol.* **15**, 550 (2014).
43. R. C. McLeay, T. L. Bailey, Motif Enrichment Analysis: A unified framework and an evaluation on ChIP data. *BMC Bioinformatics* **11**, 165 (2010).
44. A. Khan, O. Fornes, A. Stigliani, M. Gheorghe, J. A. Castro-Mondragon, R. van der Lee, A. Bessy, J. Chèneby, S. R. Kulkarni, G. Tan, D. Baranasic, D. J. Arenillas, A. Sandelin, K. Vandepoele, B. Lenhard, B. Ballester, W. W. Wasserman, F. Parcy, A. Mathelier, JASPAR 2018: Update of the open-access database of transcription factor binding profiles and its web framework. *Nucleic Acids Res.* **46**, D1284 (2018).
45. A. Jolma, J. Yan, T. Whitington, J. Toivonen, K. R. Nitta, P. Rastas, E. Morgunova, M. Enge, M. Taipale, G. Wei, K. Palin, J. M. Vaquerizas, R. Vincentelli, N. M. Luscombe, T. R. Hughes, P. Lemaire, E. Ukkonen, T. Kivioja, J. Taipale, DNA-binding specificities of human transcription factors. *Cell* **152**, 327–339 (2013).
46. C. E. Grant, T. L. Bailey, W. S. Noble, FIMO: Scanning for occurrences of a given motif. *Bioinformatics* **27**, 1017–1018 (2011).
47. C. Trapnell, D. G. Hendrickson, M. Sauvageau, L. Goff, J. L. Rinn, L. Pachter, Differential analysis of gene regulation at transcript resolution with RNA-seq. *Nat. Biotechnol.* **31**, 46–53 (2013).
48. M. D. Robinson, D. J. McCarthy, G. K. Smyth, edgeR: A Bioconductor package for differential expression analysis of digital gene expression data. *Bioinformatics* **26**, 139–140 (2010).
49. C. Y. McLean, D. Bristor, M. Hiller, S. L. Clarke, B. T. Schaar, C. B. Lowe, A. M. Wenger, G. Bejerano, GREAT improves functional interpretation of *cis*-regulatory regions. *Nat. Biotechnol.* **28**, 495–501 (2010).
50. D. W. Huang, B. T. Sherman, R. A. Lempicki, Bioinformatics enrichment tools: Paths toward the comprehensive functional analysis of large gene lists. *Nucleic Acids Res.* **37**, 1–13 (2009).
51. G. Yu, L.-G. Wang, Y. Han, Q.-Y. He, clusterProfiler: An R package for comparing biological themes among gene clusters. *OMICS* **16**, 284–287 (2012).

Acknowledgments: We thank the members of the Kreidberg and Park laboratories for valuable comments during the course of the work, F. Danesh (M.D. Anderson) for Nphs2-CreERt2 mice, V. Huff (M.D. Anderson) for Wt1 floxed mice, and M. Kann (M.D. Cologne, Germany) and B. Laurent (Sherbrooke, Canada) for advice on experimental approaches. **Funding:** This work was supported by 1R01DK109972-01 to J.A.K., DP2EB029388 and U01EB028899 to R.M., R01 DK091299-01 to V.S., and a grant from the Uehara Memorial Foundation to K.H. **Author contributions:** S.E. performed the experimental work on mice and immortalized podocytes. Y.L.J. and D.J. performed the bioinformatic analyses. T.M., K.H., and S.E. performed experimental work with human kidney organoids. S.E. and M.E.T. performed mouse husbandry. V.S. derived the immortalized podocyte cell line. R.M. supervised the human kidney organoid experiments. P.J.P. supervised the bioinformatic analyses. S.E., Y.L.J., R.M., and J.A.K. conceived the project and wrote the manuscript. P.J.P. and J.A.K. supervised the entire project. **Competing interests:** All authors declare that they have no competing interests. **Data and materials availability:** All data needed to evaluate the conclusions in the paper are present in the paper and/or the Supplementary Materials. The ChIP-seq and RNA-seq data generated for this study are deposited to GEO with accession number GSE149486.

Submitted 2 March 2020
Accepted 10 June 2020
Published 24 July 2020
10.1126/sciadv.abb5460

Citation: S. Ettou, Y. L. Jung, T. Miyoshi, D. Jain, K. Hiratsuka, V. Schumacher, M. E. Taglienti, R. Morizane, P. J. Park, J. A. Kreidberg, Epigenetic transcriptional reprogramming by WT1 mediates a repair response during podocyte injury. *Sci. Adv.* **6**, eabb5460 (2020).

ScienceAdvances

Epigenetic transcriptional reprogramming by WT1 mediates a repair response during podocyte injury

Sandrine EttouYoungsook L. JungTomoya MiyoshiDhawal JainKen HiratsukaValerie SchumacherMary E. TaglientiRyuji MorizanePeter J. ParkJordan A. Kreidberg

Sci. Adv., 6 (30), eabb5460. • DOI: 10.1126/sciadv.abb5460

Science Advances (ISSN 2375-2548) is published by the American Association for the Advancement of Science. 1200 New York Avenue NW, Washington, DC 20005. The title *Science Advances* is a registered trademark of AAAS.